# EXPLORING THE QCD PHASE DIAGRAM

Volker Koch

Nuclear Science Division, Lawrence Berkeley National Laboratory
Berkeley, CA, 94720, USA

Volodymyr Vovchenko

Physics Department, University of Houston
3507 Cullen Blvd, Houston, TX 77204, USA

*Received 27 March 2026, accepted 9 April 2026,*
*published online 28 May 2026*

Exploring the QCD phase diagram through relativistic heavy-ion collisions is a primary goal of modern nuclear physics. This contribution focuses on fluctuations and correlations of conserved charges — specifically net-baryon and net-charge cumulants — as sensitive probes of the phase structure and the QCD critical point. We discuss recent theoretical and experimental advancements, highlighting constraints from lattice QCD and new results from the RHIC Beam Energy Scan program. Key challenges in theory-to-experiment comparisons at high baryon density are discussed, alongside the systematic requirements for meaningful physical interpretation. Finally, we identify open issues and outline the discovery potential of future low-energy experiments, such as CBM, in resolving the high-density regime of the phase diagram.

DOI:10.5506/APhysPolB.57.6-A6

## 1. Introduction

One of the primary objectives in strong interaction physics is to investigate the properties of strongly interacting matter, particularly its phase structure. This is typically illustrated in the QCD phase diagram, plotted as a function of temperature $T$ and baryon chemical potential $\mu_B$.

Theoretically, the phase diagram is explored using thermal field theory, with lattice QCD providing a non-perturbative approach. Lattice calculations reveal a crossover transition from hadronic matter to quark–gluon plasma (QGP) at high temperatures and vanishing $\mu_B$ [1]. However, the fermion sign problem hinders lattice QCD at high baryon densities, where the QCD critical point (CP) and potential first-order transitions are expected [2].

Recent advancements include extrapolations from lattice data at zero or imaginary chemical potential [3–6], functional methods such as Dyson–Schwinger equations [7–9], functional renormalization group [10, 11], and effective models [12]. These converge on a CP location around 100 MeV $\lesssim T_C \lesssim$ 120 MeV and 550 MeV $\lesssim \mu_C \lesssim$ 650 MeV, corresponding roughly to $\sqrt{s_{NN}} \simeq 5$ GeV based on freeze-out systematics.

Experimentally, the QCD phase diagram is probed via high-energy heavy-ion collisions at the LHC and RHIC. At high energies, the net-baryon density at mid-rapidity is near zero, so lower beam energies are needed to achieve a finite density. The RHIC Beam Energy Scan (BES) systematically varies beam energy to map the phase diagram [13], complemented by fixed-target experiments such as NA61/SHINE [14] and HADES [15].

Key observables include fluctuations of conserved charges, especially baryon-number cumulants, which reflect derivatives of the pressure with respect to $\mu_B$ and are sensitive to phase structures such as the crossover or CP [16]. These can be computed in lattice QCD at $\mu_B = 0$, enabling theory–experiment comparisons.

Evidence for a first-order transition might come from spinodal decomposition which, due to rapid phase separation, leads to the formation of lumps of dense matter [17–19], though detecting these in experiment remains challenging [20, 21]. Electromagnetic probes like dileptons could also signal mixed-phase effects [22–24].

The upcoming CBM experiment at FAIR, targeting $\sqrt{s_{NN}} = 2.8$–$4.9$ GeV, is poised to measure high-order fluctuations in the predicted CP region with high precision.

This contribution emphasizes fluctuation and correlation observables in heavy-ion collisions, using lattice QCD and other methods to guide exploration. It is structured as follows: Section 2 covers theoretical predictions for the QCD CP. Section 3 discusses fluctuations and correlations. Section 4 compares experiments with theory. Section 5 examines non-critical baselines and data. Section 6 addresses open questions and future steps. Section 7 summarizes findings.

## 2. Theoretical predictions

As discussed in the introduction, direct lattice QCD calculations at finite baryon density are hindered by the sign problem, making it challenging to predict the location of the QCD critical point (CP) from first principles. Consequently, current predictions rely on extrapolations from lattice QCD at zero or imaginary chemical potential, or on alternative theoretical approaches.

Lattice QCD can compute baryon-number susceptibilities — derivatives of the pressure with respect to the chemical potential — at zero baryon chemical potential [29–33]. Calculations at imaginary chemical potential, which avoid the sign problem, can be analytically continued to real chemical potential [34] providing an alternative way to determine the susceptibilities. These susceptibilities enable Taylor expansions of the pressure and related observables for small $\mu_B/T \lesssim 3$, which may be extended somewhat through generalized expansion schemes [35–37]. Alternatively, one can apply a fugacity or cluster expansion [38, 39] with similar ranges of validity. However, such expansions cannot capture the non-analytic behavior associated with the CP, so their validity does not extend into the critical region.

Alternative strategies focus on observables sensitive to the CP, such as the Yang–Lee edge singularities in the complex chemical potential plane [40]. Recent lattice QCD studies use Padé approximants to locate these singularities from data at zero and imaginary chemical potential, then extrapolate their trajectories to lower temperatures [4, 5, 41]. If the singularities approach the real axis, this may indicate a CP. Current results suggest a possible CP at $T \lesssim 110$ MeV, but these analyses are subject to systematic uncertainties from finite-volume effects, lack of continuum extrapolation, and the reliability of analytic continuation. For this reason, these predictions are not yet included in Fig. 1, but the method remains promising as systematics improve.

Another recent approach [6] uses constant entropy density contours, exploiting the expected crossing of such contours at the CP. By expanding along these contours using susceptibilities and their temperature derivatives, this method can describe mean-field-type critical behavior and first-order transitions. It predicts a CP at $T \approx 114$ MeV and $\mu_B \approx 602$ MeV under $\mu_S = \mu_Q = 0$ conditions. A related analysis [42] extrapolates constant entropy density contours from imaginary to real chemical potential, ruling out a CP at $\mu_B < 450$ MeV at the $2\sigma$ level.

Holographic models provide complementary predictions. For example, an Einstein–Maxwell–Dilaton model calibrated to lattice QCD thermodynamics at $\mu_B = 0$ yields a CP at $T_C \simeq 101$–$108$ MeV and $\mu_C \simeq 560$–$625$ MeV [12]. A VQCD analysis constrained by neutron star observations finds a CP at $T_C \sim 119$ MeV and $\mu_C \sim 626$ MeV [26]. Despite differing inputs and conditions, both approaches locate the CP in a similar region.

Functional methods, such as the functional renormalization group (fRG) and Dyson–Schwinger equations (DSE), have also matured. Recent studies benchmarked to lattice QCD at $\mu_B = 0$ predict a CP at $T_C \sim 110$–$120$ MeV and $\mu_C \sim 600$–$650$ MeV [8, 10, 25], with some differences in the conditions for the chemical potentials, such as $\mu_S = \mu_B/3$ *versus* $\mu_S = 0$.

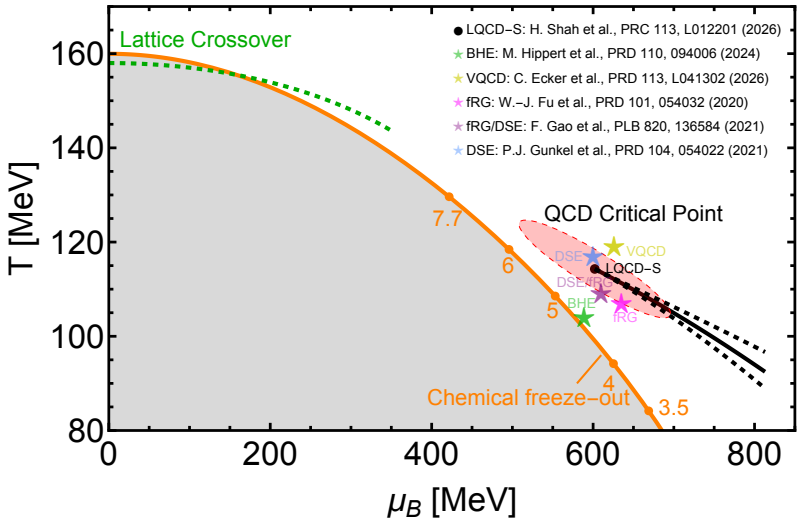


Fig. 1. Based on [6]. A compilation of predictions for the location of the QCD critical point on the $T$–$\mu_B$ phase diagram of QCD. The black point with a red covariance ellipse shows the estimate from Ref. [6], based on the extrapolation of constant entropy density contours from $\mu_B = 0$. The stars depict estimates from other approaches, functional methods (fRG [10], DSE-fRG [8], DSE [25]) and holography (BHE [12], VQCD [26]). The orange line represents the chemical freeze-out estimate from Ref. [27], with points on the line corresponding to various collision energies (in terms of $\sqrt{s_{NN}}$ in GeV). Both the chemical freeze-out line and all CP estimates [except DSE ($\mu_S = \mu_B/3$) and VQCD ($\beta$-equilibrium)] correspond to $\mu_S = 0$ ($n_S \neq 0$) conditions. The dashed green line depicts the chiral crossover line from [28].

In summary, a range of theoretical approaches increasingly converge on a region for the QCD critical point around $T_C \sim 100$–$120$ MeV and $\mu_C \sim 550$–$650$ MeV. However, these should be viewed as target regions rather than precise predictions, as each method involves different assumptions and systematic uncertainties. Alternative models, such as chiral mean-field constructions tuned to both heavy-ion and neutron star data [43], can yield qualitatively different phase structures, including a CP at much higher density. Thus, the region shown in Fig. 1 represents the most likely location based on current knowledge, but not a definitive constraint.

## 3. Correlations and fluctuations

Fluctuations and correlations serve as sensitive probes of a system's dynamics and underlying degrees of freedom. Classical examples include energy

fluctuations characterized by the heat capacity [44]. Most relevant to this review are long-range correlations near a critical point, which produce large fluctuations, as exemplified by critical opalescence [44].

Beyond mapping the phase diagram, fluctuations and correlations reveal the microscopic constituents of a system. For instance, fluctuations of net charge and baryon number in QCD are sensitive to the fractional charges carried by quarks [45–48]. Similarly, correlations between conserved charges can be used to test whether the system has undergone deconfinement [49, 50]. For an overview, see Refs. [51, 52].

As already mentioned, fluctuations of conserved charges are sensitive to the structure of the QCD phase diagram in general and the QCD critical point in particular. The reason for this is that the cumulants of the conserved charge distribution are related to the derivatives of the pressure with respect to the chemical potential. In particular, for the baryon-number cumulants, $\kappa_n[B]$, we have

$$\kappa_n[B] = \frac{\partial^n(\ln Z)}{\partial(\mu_B/T)^n} = \frac{V}{T}\frac{\partial^n P}{\partial(\mu_B/T)^n}\,. \tag{1}$$

Cumulants can also be calculated in thermal field theories such as lattice QCD. These calculations typically determine so-called susceptibilities, which are defined as

$$\chi_n[B] = \frac{\partial^n\left(P/T^4\right)}{\partial(\mu_B/T)^n}\,, \tag{2}$$

and are trivially related to the cumulants

$$\kappa_n[B] = VT^3\chi_n[B]\,. \tag{3}$$

At vanishing chemical potential, susceptibilities up to $8^{\text{th}}$ order have been extracted in lattice QCD [31, 34]. Due to the fermion sign problem, lattice QCD calculations at finite chemical potential are not possible. However, susceptibilities can be calculated at imaginary chemical potential, which can then be analytically continued to real values of the chemical potential [34]. Alternatively, they may be obtained via Taylor expansion in powers of the chemical potential. Both methods, however, are restricted to small values of the baryon-number chemical potential, $\frac{\mu_B}{T} \lesssim 3$.

Cumulants are extensive quantities that scale with system size. Because the system size in heavy-ion collisions is neither well known nor controlled, experimental measurements typically use cumulant ratios to eliminate leading-order volume dependence. This approach also enables direct comparison with lattice QCD susceptibilities, since the susceptibility ratios are identical to cumulant ratios. The most common cumulant ratios are

$$\frac{\kappa_2}{\kappa_1}\,; \qquad \frac{\kappa_3}{\kappa_2} = S\sigma\,; \qquad \frac{\kappa_4}{\kappa_2} = K\,\sigma^2\,, \tag{4}$$

where $S$, $K$, and $\sigma$ are the skewness, kurtosis, and standard deviation.

While taking the ratio removes the leading dependence on the volume, there is still the remaining effect of volume fluctuations. Even for the best centrality cuts, the impact parameter of the collisions and thus the volume of the produced systems changes from event to event [53]. As we shall discuss below, these volume fluctuations give rise to significant corrections [54–56] which need to be controlled.

At lower collision energies, where the production of anti-baryons can be neglected, it may be advantageous to study factorial cumulants $\hat{C}_k$ instead of cumulants $\kappa_k$ which are related to cumulants via

$$\hat{C}_n = \sum_{k=1}^{n} s(n,k)\kappa_k \,, \tag{5}$$

where $s(n,k)$ are the Stirling numbers of the first kind.

One important feature of factorial cumulants is that they represent integrated genuine correlation functions, *i.e.* they measure the true correlations in the system [57]. Another related property of factorial cumulants is that they measure the deviation from Poisson statistics, whereas cumulants measure the deviation from Gaussian statistics. For a Gaussian distribution, $\kappa_{k>2} = 0$, while for a Poisson distribution, $\hat{C}_n > 1 = 0$. Also, factorial cumulants, $\hat{C}_n\{p\}$, of a distribution which is folded with a binomial distribution with the Bernoulli probability $p$ are simply related to that of the original distribution, $\hat{C}_n$, via

$$\hat{C}_n\{p\} = p^n \hat{C}_n \,. \tag{6}$$

Thus, for small Bernoulli probabilities, the factorial cumulants vanish, $\hat{C}_n\{p \to 0\} \to 0$ for $n > 1$, demonstrating that for small acceptance windows, the resulting (factorial) cumulants are consistent with those of a Poisson distribution.

While cumulants are measurable experimentally and calculable in lattice QCD, direct comparison requires care, as we shall elaborate in the next section.

## 4. Comparing experiment with theory

Experiment and theory probe different systems: in experiments, charges are conserved globally (canonical ensemble), while field theory calculations assume grand-canonical conditions with average conservation only. These differences can be mitigated by studying subsystems such as rapidity slices [51], though residual corrections due to global charge conservation remain sizable [58–61]. Fortunately, such corrections are calculable for QCD [62–64], and local charge conservation effects have also been studied [65, 66].

Theory calculates baryon-number cumulants, whereas experiments typically measure only protons. At high pion multiplicities, charge-exchange reactions effectively randomize proton and neutron numbers [67, 68]. In this regime, proton cumulants relate to baryon-number cumulants through binomial folding with Bernoulli probability $p = \langle N_p \rangle / \langle N_B \rangle \simeq 1/2$, which shifts cumulants toward the Poisson (Skellam) limit.

Additionally, thermal motion causes particles in a given spatial rapidity bin to spread over a range of momentum-space rapidities. This "thermal smearing" causes observed cumulants to approach the Poisson limit as the rapidity acceptance window shrinks [69].

The left panel of Fig. 2 illustrates these corrections. It shows cumulant ratios $\kappa_4/\kappa_2$ and $\kappa_6/\kappa_2$ as functions of rapidity acceptance for an LHC system (see [70] for details). The figure displays four results: gray horizontal lines (lattice QCD values), black dashed lines (effect of global charge conservation), red lines (both conservation and thermal smearing), and blue points (net-proton cumulants including both effects). The red lines show how thermal smearing causes the ratios to approach the Poisson limit ($\kappa_4/\kappa_2 = 1$) as the acceptance window shrinks. The blue diamonds mark results using the method from [67, 68].

These predictions reveal a striking discrepancy between lattice QCD predictions and experimental observations. Assuming thermal equilibrium, the blue points show what experiments like ALICE should observe if the underlying fluctuations are those predicted by lattice QCD. Clearly, there is a significant difference between the predicted and observed values. Most notably, for the hyper-kurtosis $\kappa_6/\kappa_2$, lattice QCD predicts a negative value while net protons yield positive values. This is of importance since a negative hyper-kurtosis has been proposed as a signal of chiral criticality [71]. To extract the true underlying baryon-number signal, the aforementioned corrections need to be carefully applied, and one needs to measure several cumulant ratios across different acceptance windows to control systematic uncertainties. To date, only second-order proton cumulants have been fully measured [72, 73].

The right panel of Fig. 2 depicts the same cumulant ratios as functions of collision energy for Au–Au collisions at RHIC, evaluated using hydrodynamic model calculations [74]. Four scenarios are shown.

The dash-dotted black line represents net-baryon cumulants in the grand-canonical ensemble without momentum cuts. These show suppression relative to the Skellam baseline (unity), reflecting correlations from baryon excluded-volume interactions and agreeing with lattice QCD susceptibilities, as expected from thermal field theory.

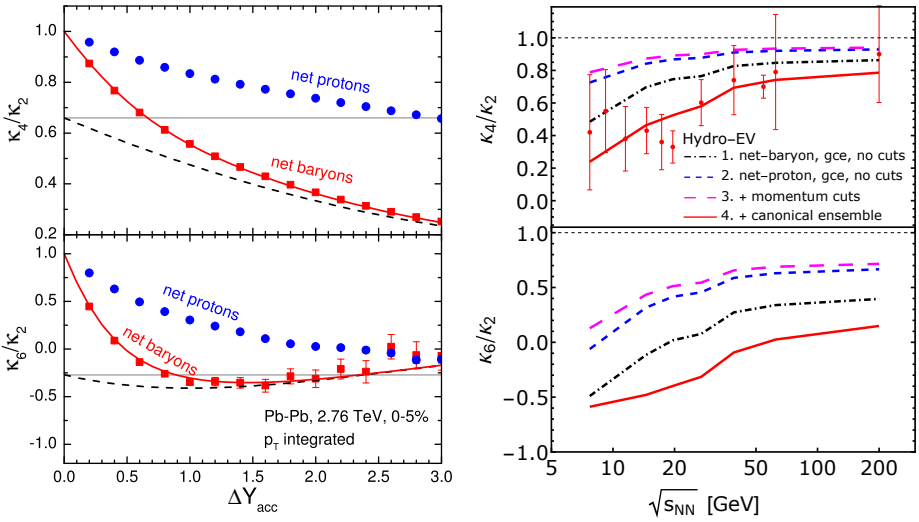


Fig. 2. Left panel: Cumulant ratios $\kappa_4/\kappa_2$ (upper panel) and $\kappa_6/\kappa_2$ (lower panel) as functions of the acceptance window in rapidity, $\Delta Y$, for a system created in heavy-ion collisions at the LHC. The horizontal gray lines represent the result from lattice QCD calculations for the net baryons [31, 34]. The black dashed lines show the effect of global charge conservation, while the red lines also include thermal smearing. The blue points are the results for the net-proton cumulant ratio, again with charge conservation and thermal smearing included. The blue diamonds are the results for net-proton cumulants using the method of [67, 68]. For details, see [70], where this figure is adapted from. Right panel: Cumulant ratios $\kappa_4/\kappa_2$ (upper panel) and $\kappa_6/\kappa_2$ (lower panel) as functions of collision energy for RHIC-BES collider energies for a fixed rapidity window. Hydro-EV model calculations from [74] depicting cumulant ratios of *(i)* net baryons in the grand-canonical ensemble without momentum cuts (dash-dotted black line), *(ii)* the same but for net protons (dashed blue line), *(iii)* net protons with momentum cuts (dashed magenta line), and *(iv)* net protons with momentum cuts and baryon-number conservation effects included (solid red line).

Switching to net protons (dashed blue line) and applying no momentum cuts shifts the cumulants significantly closer to the Skellam baseline, reflecting missing neutrons that dilute baryon correlations. Adding momentum cuts (dashed magenta line) further reduces the signal.

Remarkably, when baryon-number conservation is included (solid red line), the net-proton cumulants swing back away from the Skellam baseline, approaching values closer to the grand-canonical net-baryon case. This interplay between several competing effects may explain why net-baryon susceptibilities from lattice QCD (grand-canonical, no cuts) happen to agree

reasonably well with measured net-proton cumulant ratios (canonical, with cuts) despite corresponding to different observables (baryons *versus* protons). These results underscore the need for caution when comparing lattice QCD susceptibilities with experimental cumulant ratios.

There are additional effects which have not been taken into account in the calculations shown in Fig. 2. One is the so-called volume fluctuations, which arise from the event-by-event fluctuations of the impact parameter, which persist even with the tightest centrality cuts. These affect the measured value of the cumulants [56]. The STAR Collaboration applies so-called centrality bin width corrections (CBWC) [75] to suppress volume fluctuations. However, the magnitude of these corrections is not fully controlled [76]. An alternative approach based on mixed events [77] does not remove all effects either, but the method provides an estimate for the bias, which can be constrained by the systematics of the system under investigation. This bias is parametrically suppressed for systems with large charged-particle multiplicities, which, unfortunately is not the situation for the energies where the critical point is expected. Therefore, one needs to either rely on simulations or develop and measure so-called strongly intensive observables [78, 79] which are not affected by volume fluctuations. Also, a new method based on the Edgeworth expansion [80] has recently been proposed, which is claimed to be able to determine the cumulants without a specific centrality selection.

These equilibrium-based effects are all studied for static systems. However, systems created in heavy-ion collisions are inherently dynamic. If the system's evolution is governed by hydrodynamics and the hydrodynamic scales are larger than the critical correlation length [81], local thermal equilibrium may provide a reasonable description. To calculate critical fluctuation effects, diffusion and non-hydrodynamic modes must also be propagated. This can be accomplished either via stochastic hydrodynamics [82] or by explicitly tracking two- and higher-order critical correlation functions as proposed in [81]. At the end of hydrodynamic evolution, these correlations and fluctuations need to be converted into particle numbers, recent maximum entropy freeze-out provides a pathway to doing that [83].

At lower collision energies, non-equilibrium effects may become important, making hydrodynamic approaches unreliable. A proper treatment would require kinetic theory tailored for QCD matter, which remains undeveloped. Nonetheless, insights can be gained from classical systems. Recent studies [84, 85] examined a Lennard-Jones fluid (which shares the same critical universality class as QCD) using molecular dynamics to illuminate key differences between theory and experiment.

This study also addressed another important aspect: experiments measure in momentum space (integrating over spatial coordinates), while theory typically calculates in spatial coordinates (integrating over all momenta).

Consequently, a small subsystem in experiment is defined by momentum cuts, whereas in theory, it results from spatial cuts. For a Lennard-Jones fluid with interactions $V(x_i, x_j) = V(|x_i - x_j|)$, the partition function

$$\begin{aligned} Z &= \int_{\Omega} \mathrm{d}x_1 \mathrm{d}p_1 \cdots \mathrm{d}x_N \mathrm{d}p_N \exp\left(-\frac{H}{T}\right) \\ &= \int_{\Delta P} \mathrm{d}p_1 \cdots \mathrm{d}p_N \exp\left(-\frac{\sum_i p_i^2}{2mT}\right) \\ &\quad \times \int_{\Delta R} \mathrm{d}x_1 \cdots \mathrm{d}x_N \exp\left(\frac{-\sum_{i,j} V(x_i, x_j)}{T}\right) \\ &= Z_P Z_R \end{aligned} \tag{7}$$

factorizes into momentum ($Z_P$) and spatial ($Z_R$) contributions. Selecting particles by momentum cuts samples $Z_P$ (essentially a non-interacting gas), missing correlations entirely. In contrast, spatial cuts sample $Z_R$, capturing interaction-induced correlations. Thus for a static, non-expanding system measurements in momentum space will not exhibit critical signals as demonstrated in [84, 85]. However, in heavy-ion collisions, collective flow

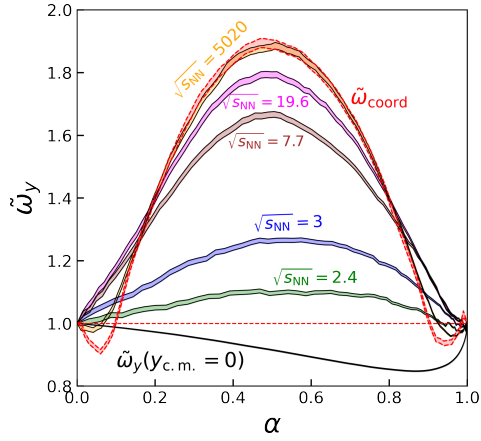


Fig. 3. Corrected scaled variance $\tilde{\omega}_y$ of particle number in rapidity acceptance as a function of the fixed acceptance fraction $\alpha_y$, which is the ratio of accepted to total number of particles. Calculations are performed for a system of $N = 400$ particles at $T = 1.06T_c$ and $n = 0.95n_c$. Different bands correspond to different magnitudes of the collective flow corresponding to the collision energies in a Bjorken picture. The limiting cases of coordinate, red band, labeled $\tilde{\omega}_{\mathrm{coord}}$, and rapidity acceptance, black line, labeled $\tilde{\omega}_y(y_{\mathrm{cm}} = 0)$, in the absence of collective expansion are also shown. For details, see [85] where this figure is adapted from.

correlates momentum and coordinate space, allowing momentum cuts to indirectly probe spatial correlations. Still, at lower energies with weaker flow, critical signals may be significantly reduced [85]. This is illustrated in Fig. 3, where the scaled variance of particle number is shown as a function of the acceptance fraction for different flow strengths corresponding to various collision energies. The signal without flow (black line) corresponds to a non-interacting gas in the micro-canonical ensemble, while the signal obtained in coordinate space (red line) represents typical theoretical predictions. As flow increases with collision energy, the scaled variance approaches the coordinate space result, but at lower energies ($\sqrt{s_{NN}} \simeq 3$–$7$ GeV), where the CP is predicted, the signal is significantly reduced.

## 5. Non-critical baselines

Ideally, one would have a theoretical model describing the entire dynamical evolution of heavy-ion collisions with phase transition effects, but no such model currently exists, though developments are underway [81, 86, 87]. But even with such a model at hand, it is essential to develop a non-critical baseline: a model with all known physics except correlations from QCD critical points or phase transitions. Deviations reveal where New Physics emerges. Effective baselines incorporate the corrections discussed in Section 4 (baryon conservation, thermal smearing, *etc.*) and ideally reproduce other observables like particle spectra.

Three main approaches exist: *(i)* UrQMD [88–90] conserves charges, includes thermal smearing, provides both proton and baryon cumulants, and permits identical experimental cuts and centrality bin width corrections [89]; *(ii)* Hadron Resonance Gas (HRG-CE) [91] incorporates global charge conservation and experimental constraints; *(iii)* Viscous Hydrodynamics (Hydro-EV) [74] uses hydrodynamics tuned to spectra with particlization respecting baryon conservation [64]. Excluded-volume corrections are tuned to match lattice QCD cumulants at $\mu_B = 0$ [38, 92]. Both, HRG-CE and Hydro-EV include thermal smearing and provide results for both (net)-protons and (net)-baryons. However, neither accounts for volume fluctuations but STAR's centrality bin width corrections may mitigate this issue [76].

Figure 4 compares recent STAR data from RHIC BES-II (factorial) cumulants with three non-critical baselines: Hadron Resonance Gas (HRG-CE) [91] (dotted black line), hydrodynamics with eigenvolume corrections (Hydro-EV) [74] (blue dashed line), and UrQMD simulations carried out by the STAR Collaboration (yellow band). The HRG-CE and Hydro-EV results were obtained prior to the data release, serving as genuine theoretical predictions; they apply to the central data (red squares).

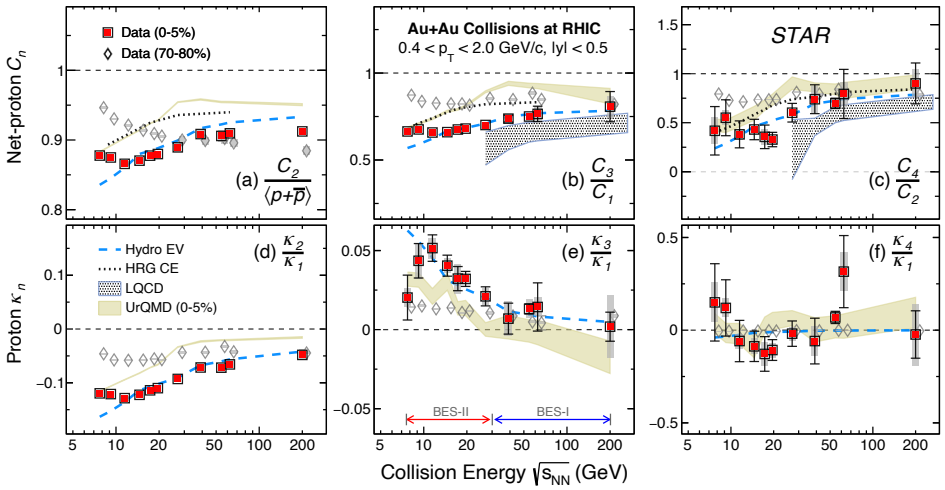


Fig. 4. Cumulants (top row) and factorial cumulants (bottom row) obtained by the STAR Collaboration from the second phase of the RHIC beam energy scan [90]. Note that, contrary to common practice, STAR uses $C_n$ to denote cumulants and $\kappa_n$ to denote factorial cumulants. Also shown are the baselines of [74] (blue dashed line, denoted as Hydro-EV in the text), [91] (dotted black line, denoted as HRG-CE in the text) as well as UrQMD calculations by STAR (brown band). Also shown are lattice QCD results for net baryons uncorrected for global baryon-number conservation [33]. Figure adapted from [90].

All three baselines successfully reproduce the overall trend of the data *versus* collision energy. Notably, the Hydro-EV baseline agrees quantitatively with the measurements (within errors) for collision energies above $\sqrt{s_{NN}} \gtrsim 10$ GeV. However, a striking discrepancy emerges at the lowest two collision energies: while the Hydro-EV baseline continues to decrease (increase) monotonically for the second (third) order factorial cumulants, the data show a clear non-monotonic behavior. This anomalous trend extends to even lower energies, where STAR reports further enhanced (diminished) second (third) order factorial cumulants at $\sqrt{s_{NN}} = 3$ GeV [89].

The essential difference between Hydro-EV and HRG-CE lies in the eigenvolume correction, which physically represents a short-range repulsion among baryons. At lower collision energies, the observed trends suggest two possibilities: either the repulsion diminishes or it becomes outweighed by an attractive force to reconcile with the lowest two energy points, where HRG-CE matches the data better. A recent model calculation [93] shows that in principle, interactions are able to reproduce the data (see Fig. 5). However, in this model, the interaction acts in momentum space and the parameters are tuned to fit the data. Also, no relation to any known interaction has yet

been established. We note that the interplay of attractive and repulsive interactions commonly leads to the existence of a phase transition and critical dynamics [94].

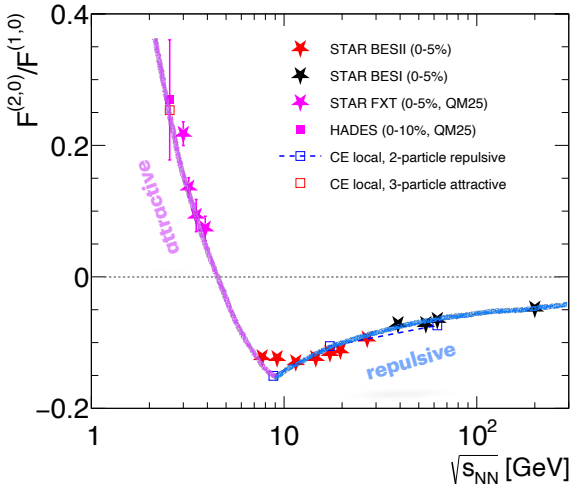


Fig. 5. Energy dependence of the second-order factorial cumulant obtained by including repulsive (blue line) and attractive (red line) momentum space interactions as calculated in [93]. The data points are from the STAR and HADES collaborations. Figure adapted from [93].

Of course, the observed behavior may reflect well-established nuclear interactions, which inherently combine short-range repulsion with long-range attraction. These interactions are responsible for the nuclear liquid–gas phase transition and its associated critical point. Indeed, model calculations of equilibrium fluctuations along the freeze-out line show that the nuclear liquid–gas phase transition itself contributes substantially to cumulants at low and intermediate collision energies [95–97]. To what extent these interactions can explain the observed behavior in the data, however, needs to be further investigated.

A third possibility involves volume fluctuations, a more prosaic effect unrelated to critical dynamics. A recent study [98] used UrQMD simulations without mean-field interactions to examine how impact parameter variations affect cumulants. Two scenarios were compared: *(i)* restricted impact parameter range ($b < 3$ fm) and *(ii)* STAR's standard centrality selection. Figure 6 (right panel) shows factorial cumulants for symmetric rapidity acceptance ($-0.5 < y < 0.5$). At fixed impact parameter, the energy dependence is minimal (blue crosses). In contrast, applying STAR's centrality selection (red squares) produces the observed trend: second-order

factorial cumulants rise at lower energies, while third-order values drop — matching experimental data. Both cases included centrality bin width corrections (CBWC).

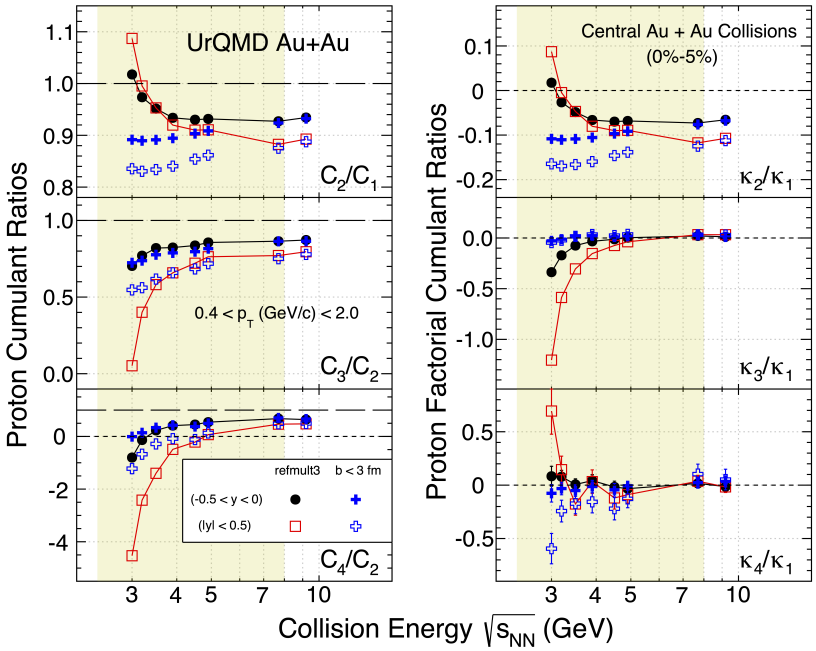


Fig. 6. Energy dependence of cumulants (left panel) and factorial cumulants (right panel) obtained from UrQMD simulations [98] for different rapidity acceptance windows and for fixed impact parameter (blue crosses) and centrality selection à la STAR (red square and black filled circle). Figure adapted from [98].

Restricting the impact parameter range substantially suppresses participant fluctuations, yielding energy-dependence patterns similar to HRG-CE and Hydro-EV — models that ignore volume effects. The energy dependence observed in the actual data may therefore arise primarily from volume fluctuations, which may persist in STAR's centrality selection despite CBWC corrections. At higher energies ($\sqrt{s_{NN}} \gtrsim 7$ GeV), where particle multiplicities are large, centrality selection effects diminish, and CBWC successfully removes volume-fluctuation artifacts as shown in [76]. Also, at the 2025 Quark Matter conference, STAR presented their data on the beam energy dependence of (factorial) cumulants together with results from UrQMD simulations (without any mean-field interactions) using the same centrality selection as in the data and applying the same CBWC procedure [99]. They find that the UrQMD calculations qualitatively reproduce the observed non-monotonic trend in the data. Clearly, this issue needs further investigation

before any conclusions about additional, potentially critical dynamics can be drawn, in particular in view of the upcoming CBM experiment which will measure in the region where the QCD critical point is predicted to be located.

## 6. Open issues and next steps

The various baselines discussed in the previous section give the correct trend and in one case even a quantitative agreement with the energy dependence of the measured (factorial) cumulants for energies above $\sqrt{s_{NN}} \gtrsim 10$ GeV. These baselines take into account the essential "trivial" effects discussed in Section 4, baryon-number conservation and the fact that only protons, and not all baryons, are measured and, in the case of UrQMD, also volume fluctuations. In order to see if there is potentially additional physics, it would be good to provide an additional observable which tests these baselines and their assumptions. Such an observable has been recently put forward in [100]. Specifically, the authors propose to look at the acceptance dependence on the reduced correlation coefficients or couplings defined as [101–103]

$$\hat{c}_n = \frac{\hat{C}_n}{\langle N \rangle^n}\,, \tag{8}$$

where $\langle N \rangle = \kappa_1 = \hat{C}_1$ is the mean number of protons. Since global baryon-number conservation, protons *versus* baryons, as well as volume fluctuations lead only to global and thus long-range correlations, Ref. [100] shows that in that case, the reduced correlation coefficients will be constant as a function of the size of the rapidity window. In addition to the above scaling of the factorial cumulants, the ratio of the second-order reduced correlation coefficients for protons and anti-protons are found to be virtually identical for an ideal hadron gas in the grand-canonical ensemble, which underlies both the HRG-CE and Hydro-EV baselines, $\hat{c}_2[p] = \hat{c}_2[\bar{p}]$. The authors of Ref. [100] find that the above scaling is consistent within the rather large errors with the data for STAR data from the first phase of the beam energy scan, BES I, and for energies up to $\sqrt{s_{NN}} \simeq 27$ GeV, the prediction of [74] agrees quantitatively for the proton correlation coefficient. However, there is a significant difference between the reduced correlation coefficients for protons and anti-protons, which is not expected from the baselines. As shown in Fig. 7, the difference $\hat{c}_2[p] - \hat{c}_2[\bar{p}]$ increases with decreasing collision energy.

Should the new, high-statistics data from BES II confirm these results, there is clearly a need to either revise the baseline(s) or understand possible New Physics which is beyond baryon-number conservation *etc.* One such idea put forward in Ref. [100] is a simple two-source model, which differentiates between produced protons and anti-protons and protons that are

stopped. As can be seen from the black line in Fig. 7, this model leads to the observed increase in the difference between the coupling for protons and anti-protons, but quantitatively overpredicts the data. Certainly, such a model is too simple, but it may suggest that stopping effects may be important at lower energies, implying that the picture of a single fireball may be too simplistic for collisions at lower energies.

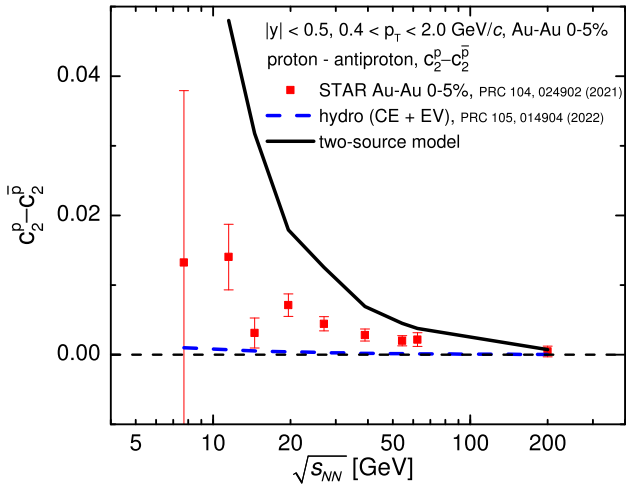


Fig. 7. Energy dependence of the difference of reduced correlation coefficients for protons and anti-protons [100] for the Hydro-EV baseline [74] (blue dashed line) and from the two-source model (black line). Figure adapted from [100].

The above discussion illustrates the need for more differential data from BES II. For example, the second-order (factorial) cumulants are related to integrals of proton–proton rapidity correlations [57], such as the ones measured by the STAR Collaboration [88] during BES I. Just as for the reduced correlation coefficients, one would expect that effects due to volume fluctuations will not affect the shape of these correlation functions. Of course, one needs to ensure that the experimental conditions such as acceptance cuts, efficiency corrections *etc.* are identical for both measurements for such a comparison to be meaningful. The same information can also be extracted from balance functions [104–106] with similar caveats about experimental conditions. Furthermore, it would be desirable to have data for all energies available from the fixed target mode, even though their interpretation will be more difficult since they will not have symmetric rapidity acceptance compared to those from collider measurements. This is not only important to understand the present results and their systematics, but it will also be crucial in preparation for the results from the upcoming CBM experiment.

Beyond cumulant measurements, several complementary observables deserve investigation: transverse momentum fluctuations [107, 108], light-nuclei yields and their fluctuations [109, 110], electromagnetic signals [111], and finite-size scaling analyses [112, 113]. A consistent signal across multiple independent observables would substantially strengthen any claim of critical behavior.

If the QCD critical point exists as predicted, collisions below $\sqrt{s_{NN}} \simeq 5$ GeV should exhibit the first-order phase transition and accompanying spinodal decomposition. While initial searches [20, 21] failed to identify clear signatures, more sophisticated methods — including machine learning approaches — offer renewed potential for detection.

## 7. Summary

Significant progress has been made toward locating the QCD critical point. On the theory side, multiple computational approaches seem to converge on a region for the location of the critical point, which should be accessible at collision energies around $\sqrt{s_{NN}} \simeq 5$ GeV.

Experimentally, STAR has delivered high-quality proton cumulant data from RHIC BES-II. Non-critical baselines have been established that successfully describe the data above $\sqrt{s_{NN}} \gtrsim 10$ GeV, making a critical point below $\mu_B \lesssim 400$ MeV unlikely.

Yet a clear puzzle emerges: at the lowest two energies (9 and 7.7 GeV), the data exhibit non-monotonic behavior in the second- and third-order factorial cumulants — a feature that baseline models do not reproduce. This anomalous trend could signal attractive interactions and incipient critical dynamics. However, mundane effects, such as volume and impact-parameter fluctuations, grow more prominent at lower energies and may equally explain the observed pattern. Distinguishing between these possibilities requires careful investigation as the energy regime of the predicted critical point is explored.

The immediate path forward is clear: upcoming fixed-target data will provide crucial tests, while the CBM experiment will directly probe the predicted critical-point region. These complementary measurements will either reveal signatures of QCD criticality or significantly constrain its location and nature.

This material is based upon work supported by the U.S. Department of Energy, Office of Science, Office of Nuclear Physics, under contract numbers DE-AC02-05CH11231 and DE-SC0026065.

## REFERENCES


[1] Y. Aoki *et al.*, «The order of the quantum chromodynamics transition predicted by the standard model of particle physics», *Nature* **443**, 675 (2006), arXiv:hep-lat/0611014.

[2] M.A. Stephanov, «QCD Phase Diagram and the Critical Point», *Prog. Theor. Phys. Suppl.* **153**, 139 (2004), arXiv:hep-ph/0402115.

[3] P. Dimopoulos *et al.*, «Contribution to understanding the phase structure of strong interaction matter: Lee–Yang edge singularities from lattice QCD», *Phys. Rev. D* **105**, 034513 (2022), arXiv:2110.15933 [hep-lat].

[4] G. Basar, «QCD critical point, Lee–Yang edge singularities, and Padé resummations», *Phys. Rev. C* **110**, 015203 (2024), arXiv:2312.06952 [hep-th].

[5] D.A. Clarke *et al.*, «Searching for the QCD critical endpoint using multi-point Padé approximations», *Phys. Rev. D* **112**, L091504 (2025), arXiv:2405.10196 [hep-lat].

[6] H. Shah *et al.*, «Locating the QCD critical point through contours of constant entropy density», *Phys. Rev. C* **113**, L012201 (2026), arXiv:2410.16206 [hep-ph].

[7] C.S. Fischer, J. Luecker, C.A. Welzbacher, «Locating the critical end point of QCD», *Nucl. Phys. A* **931**, 774 (2014), arXiv:1410.0124 [hep-ph].

[8] F. Gao, J.M. Pawlowski, «Chiral phase structure and critical end point in QCD», *Phys. Lett. B* **820**, 136584 (2021), arXiv:2010.13705 [hep-ph].

[9] J. Bernhardt, C.S. Fischer, P. Isserstedt, B.-J. Schaefer, «Critical endpoint of QCD in a finite volume», *Phys. Rev. D* **104**, 074035 (2021), arXiv:2107.05504 [hep-ph].

[10] W.-j. Fu, J.M. Pawlowski, F. Rennecke, «QCD phase structure at finite temperature and density», *Phys. Rev. D* **101**, 054032 (2020), arXiv:1909.02991 [hep-ph].

[11] W.-j. Fu *et al.*, «Ripples of the QCD critical point», *Phys. Rev. D* **111**, L031502 (2025), arXiv:2308.15508 [hep-ph].

[12] M. Hippert *et al.*, «Bayesian location of the QCD critical point from a holographic perspective», *Phys. Rev. D* **110**, 094006 (2024), arXiv:2309.00579 [nucl-th].

[13] A. Bzdak *et al.*, «Mapping the phases of quantum chromodynamics with beam energy scan», *Phys. Rep.* **853**, 1 (2020), arXiv:1906.00936 [nucl-th].

[14] NA61/SHINE Collaboration (H. Adhikary *et al.*), «Search for a critical point of strongly-interacting matter in central $^{40}$Ar+$^{45}$Sc collisions at 13 $A$–75 $A$ GeV/$c$ beam momentum», *Eur. Phys. J. C* **84**, 741 (2024), arXiv:2401.03445 [nucl-ex].

[15] HADES Collaboration (J. Adamczewski-Musch *et al.*), «Proton-number fluctuations in $\sqrt{s_{NN}} = 2.4$ GeV Au+Au collisions studied with the High-Acceptance DiElectron Spectrometer (HADES)», *Phys. Rev. C* **102**, 024914 (2020), arXiv:2002.08701 [nucl-ex].

[16] M.A. Stephanov, «Non-Gaussian Fluctuations near the QCD Critical Point», *Phys. Rev. Lett.* **102**, 032301 (2009), arXiv:0809.3450 [hep-ph].

[17] J. Randrup, «Spinodal Decomposition during the Hadronization Stage at RHIC?», *Phys. Rev. Lett.* **92**, 122301 (2004), arXiv:hep-ph/0308271.

[18] J. Randrup, «Phase transition dynamics for baryon-dense matter», *Phys. Rev. C* **79**, 054911 (2009), arXiv:0903.4736 [nucl-th].

[19] J. Steinheimer, J. Randrup, «Spinodal Amplification of Density Fluctuations in Fluid-Dynamical Simulations of Relativistic Nuclear Collisions», *Phys. Rev. Lett.* **109**, 212301 (2012), arXiv:1209.2462 [nucl-th].

[20] J. Steinheimer, J. Randrup, V. Koch, «Non-equilibrium phase transition in relativistic nuclear collisions: Importance of the equation of state», *Phys. Rev. C* **89**, 034901 (2014), arXiv:1311.0999 [nucl-th].

[21] J. Steinheimer *et al.*, «A machine learning study to identify spinodal clumping in high energy nuclear collisions», *J. High Energy Phys.* **2019**, 122 (2019), arXiv:1906.06562 [nucl-th].

[22] R. Rapp, H. van Hees, «Thermal dileptons as fireball thermometer and chronometer», *Phys. Lett. B* **753**, 586 (2016), arXiv:1411.4612 [hep-ph].

[23] F. Seck *et al.*, «Dilepton signature of a first-order phase transition», *Phys. Rev. C* **106**, 014904 (2022), arXiv:2010.04614 [nucl-th].

[24] O. Savchuk *et al.*, «Enhanced dilepton emission from a phase transition in dense matter», *J. Phys. G: Nucl. Part. Phys.* **50**, 125104 (2023), arXiv:2209.05267 [nucl-th].

[25] P.J. Gunkel, C.S. Fischer, «Locating the critical endpoint of QCD: Mesonic backcoupling effects», *Phys. Rev. D* **104**, 054022 (2021), arXiv:2106.08356 [hep-ph].

[26] C. Ecker, N. Jokela, M. Järvinen, «Locating the QCD critical point with neutron-star observations», *Phys. Rev. D* **113**, L041302 (2026), arXiv:2506.10065 [astro-ph.HE].

[27] A. Lysenko, M.I. Gorenstein, R. Poberezhniuk, V. Vovchenko, «Chemical freeze-out curve in heavy-ion collisions and the QCD critical point», *Phys. Rev. C* **111**, 054903 (2025), arXiv:2408.06473 [nucl-th].

[28] S. Borsanyi *et al.*, «QCD Crossover at Finite Chemical Potential from Lattice Simulations», *Phys. Rev. Lett.* **125**, 052001 (2020), arXiv:2002.02821 [hep-lat].

[29] S. Borsányi *et al.*, «QCD equation of state at nonzero chemical potential: continuum results with physical quark masses at order $\mu^2$», *J. High Energy Phys.* **2012**, 053 (2012), arXiv:1204.6710 [hep-lat].

[30] R. Bellwied *et al.*, «Fluctuations and correlations in high temperature QCD», *Phys. Rev. D* **92**, 114505 (2015), arXiv:1507.04627 [hep-lat].

[31] A. Bazavov *et al.*, «The QCD equation of state $\mathcal{O}(\mu_B^6)$ to from lattice QCD», *Phys. Rev. D* **95**, 054504 (2017), arXiv:1701.04325 [hep-lat].

[32] HotQCD Collaboration (A. Bazavov *et al.*), «Skewness and kurtosis of net baryon-number distributions at small values of the baryon chemical potential», *Phys. Rev. D* **96**, 074510 (2017), arXiv:1708.04897 [hep-lat].

[33] HotQCD Collaboration (A. Bazavov *et al.*), «Skewness, kurtosis, and the fifth and sixth order cumulants of net baryon-number distributions from lattice QCD confront high-statistics STAR data», *Phys. Rev. D* **101**, 074502 (2020), arXiv:2001.08530 [hep-lat].

[34] S. Borsanyi *et al.*, «Higher order fluctuations and correlations of conserved charges from lattice QCD», *J. High Energy Phys.* **2018**, 205 (2018), arXiv:1805.04445 [hep-lat].

[35] S. Borsányi *et al.*, «Lattice QCD Equation of State at Finite Chemical Potential from an Alternative Expansion Scheme», *Phys. Rev. Lett.* **126**, 232001 (2021), arXiv:2102.06660 [hep-lat].

[36] M. Kahangirwe *et al.*, «Convergence properties of the $T'$-expansion scheme: Hadron resonance gas and the cluster expansion model», *Phys. Rev. D* **111**, 094034 (2025), arXiv:2408.04588 [nucl-th].

[37] A. Abuali *et al.*, «New 4D lattice QCD equation of state: Extended density coverage from a generalized $T'$ expansion», *Phys. Rev. D* **112**, 054502 (2025), arXiv:2504.01881 [hep-lat].

[38] V. Vovchenko, J. Steinheimer, O. Philipsen, H. Stoecker, «Cluster expansion model for QCD baryon number fluctuations: No phase transition at $\mu_B/T < \pi$», *Phys. Rev. D* **97**, 114030 (2018), arXiv:1711.01261 [hep-ph].

[39] R. Bellwied *et al.*, «Corrections to the hadron resonance gas from lattice QCD and their effect on fluctuation-ratios at finite density», *Phys. Rev. D* **104**, 094508 (2021), arXiv:2102.06625 [hep-lat].

[40] V.V. Skokov, «Two lectures on Yang–Lee edge singularity and analytic structure of QCD equation of state», *SciPost Phys. Lect. Notes* **91**, 1 (2025), arXiv:2411.02663 [hep-ph].

[41] A. Adam *et al.*, «High-precision baryon number cumulants from lattice QCD in a finite box: cumulant ratios, Lee–Yang zeros and critical endpoint predictions», arXiv:2507.13254 [hep-lat].

[42] S. Borsányi *et al.*, «Lattice QCD constraints on the critical point from an improved precision equation of state», *Phys. Rev. D* **112**, L111505 (2025), arXiv:2502.10267 [hep-lat].

[43] J. Steinheimer *et al.*, «Simultaneous description of high density QCD matter in heavy ion collisions and neutron star observations», *Phys. Lett. B* **867**, 139605 (2025), arXiv:2501.12849 [hep-ph].

[44] L.D. Landau, E.M. Lifshitz, «Statistical Physics, Part 1», vol. 5 of «Course of Theoretical Physics», *Butterworth-Heinemann*, Oxford 1980, 3rd ed.

[45] M. Asakawa, U.W. Heinz, B. Müller, «Fluctuation Probes of Quark Deconfinement», *Phys. Rev. Lett.* **85**, 2072 (2000), arXiv:hep-ph/0003169.

[46] S. Jeon, V. Koch, «Charged Particle Ratio Fluctuation as a Signal for Quark–Gluon Plasma», *Phys. Rev. Lett.* **85**, 2076 (2000), arXiv:hep-ph/0003168.

[47] S. Ejiri, F. Karsch, K. Redlich, «Hadronic fluctuations at the QCD phase transition», *Phys. Lett. B* **633**, 275 (2006), arXiv:hep-ph/0509051.

[48] J. Parra *et al.*, «Indications for freeze-out of charge fluctuations in the quark–gluon plasma at the LHC», *Phys. Rev. Lett.* **135**, 242302 (2025), arXiv:2504.02085 [hep-ph].

[49] V. Koch, A. Majumder, J. Randrup, «Baryon-Strangeness Correlations: A Diagnostic of Strongly Interacting Matter», *Phys. Rev. Lett.* **95**, 182301 (2005), arXiv:nucl-th/0505052.

[50] A. Majumder, B. Müller, «Baryonic strangeness and related susceptibilities in QCD», *Phys. Rev. C* **74**, 054901 (2006), arXiv:nucl-th/0605079.

[51] V. Koch, «Hadronic Fluctuations, Correlations», in: R. Stock (Ed.) «Relativistic Heavy Ion Physics», *Springer*, 2010, pp. 626–652, arXiv:0810.2520 [nucl-th].

[52] M. Asakawa, M. Kitazawa, «Fluctuations of conserved charges in relativistic heavy ion collisions: An introduction», *Prog. Part. Nucl. Phys.* **90**, 299 (2016), arXiv:1512.05038 [nucl-th].

[53] S.J. Das, G. Giacalone, P.-A. Monard, J.-Y. Ollitrault, «Relating centrality to impact parameter in nucleus–nucleus collisions», *Phys. Rev. C* **97**, 014905 (2018), arXiv:1708.00081 [nucl-th].

[54] S. Jeon, V. Koch, «Fluctuations of Particle Ratios and the Abundance of Hadronic Resonances», *Phys. Rev. Lett.* **83**, 5435 (1999), arXiv:nucl-th/9906074.

[55] S. Jeon, V. Koch, «Event-by-Event Fluctuations», in: R.C. Hwa, X.N. Wang (Eds.) «Quark–Gluon Plasma 3», *World Scientific*, 2004, pp. 430–490, arXiv:hep-ph/0304012.

[56] V. Skokov, B. Friman, K. Redlich, «Volume fluctuations and higher-order cumulants of the net baryon number», *Phys. Rev. C* **88**, 034911 (2013), arXiv:1205.4756 [hep-ph].

[57] A. Bzdak, V. Koch, N. Strodthoff, «Cumulants and correlation functions *versus* the QCD phase diagram», *Phys. Rev. C* **95**, 054906 (2017), arXiv:1607.07375 [nucl-th].

[58] A. Bzdak, V. Koch, V. Skokov, «Baryon number conservation and the cumulants of the net proton distribution», *Phys. Rev. C* **87**, 014901 (2013), arXiv:1203.4529 [hep-ph].

[59] P. Braun-Munzinger, A. Rustamov, J. Stachel, «Bridging the gap between event-by-event fluctuation measurements and theory predictions in relativistic nuclear collisions», *Nucl. Phys. A* **960**, 114 (2017), arXiv:1612.00702 [nucl-th].

[60] O. Savchuk, R.V. Poberezhnyuk, V. Vovchenko, M.I. Gorenstein, «Binomial acceptance corrections for particle number distributions in high-energy reactions», *Phys. Rev. C* **101**, 024917 (2020), arXiv:1911.03426 [hep-ph].

[61] C.A. Pruneau, «Role of baryon number conservation in measurements of fluctuations», *Phys. Rev. C* **100**, 034905 (2019), arXiv:1903.04591 [nucl-th].

[62] V. Vovchenko *et al.*, «Connecting fluctuation measurements in heavy-ion collisions with the grand-canonical susceptibilities», *Phys. Lett. B* **811**, 135868 (2020), arXiv:2003.13905 [hep-ph].

[63] V. Vovchenko, R.V. Poberezhnyuk, V. Koch, «Cumulants of multiple conserved charges and global conservation laws», *J. High Energy Phys.* **2020**, 089 (2020), arXiv:2007.03850 [hep-ph].

[64] V. Vovchenko, «Correcting event-by-event fluctuations in heavy-ion collisions for exact global conservation laws with the generalized subensemble acceptance method», *Phys. Rev. C* **105**, 014903 (2022), arXiv:2106.13775 [hep-ph].

[65] P. Braun-Munzinger, K. Redlich, A. Rustamov, J. Stachel, «The imprint of conservation laws on correlated particle production», *J. High Energy Phys.* **2024**, 113 (2024), arXiv:2312.15534 [nucl-th].

[66] V. Vovchenko, «Density correlations under global and local charge conservation», *Phys. Rev. C* **110**, L061902 (2024), arXiv:2409.01397 [hep-ph].

[67] M. Kitazawa, M. Asakawa, «Revealing baryon number fluctuations from proton number fluctuations in relativistic heavy ion collisions», *Phys. Rev. C* **85**, 021901 (2012), arXiv:1107.2755 [nucl-th].

[68] M. Kitazawa, M. Asakawa, «Relation between baryon number fluctuations and experimentally observed proton number fluctuations in relativistic heavy ion collisions», *Phys. Rev. C* **86**, 024904 (2012), arXiv:1205.3292 [nucl-th]; *Erratum ibid.* **86**, 069902 (2012).

[69] B. Ling, M.A. Stephanov, «Acceptance dependence of fluctuation measures near the QCD critical point», *Phys. Rev. C* **93**, 034915 (2016), arXiv:1512.09125 [nucl-th].

[70] V. Vovchenko, V. Koch, «Particlization of an interacting hadron resonance gas with global conservation laws for event-by-event fluctuations in heavy-ion collisions», *Phys. Rev. C* **103**, 044903 (2021), arXiv:2012.09954 [hep-ph].

[71] B. Friman *et al.*, (Eds.) «The CBM Physics Book: Compressed Baryonic Matter in Laboratory Experiments», Lecture Notes in Physics, Vol. 814, *Springer-Verlag*, Berlin, Heidelberg 2011.

[72] ALICE Collaboration (S. Acharya *et al.*), «Global baryon number conservation encoded in net-proton fluctuations measured in Pb–Pb collisions at $\sqrt{s_{NN}} = 2.76$ TeV», *Phys. Lett. B* **807**, 135564 (2020), arXiv:1910.14396 [nucl-ex].

[73] ALICE Collaboration (S. Acharya *et al.*), «Closing in on critical net-baryon fluctuations at LHC energies: Cumulants up to third order in Pb–Pb collisions», *Phys. Lett. B* **844**, 137545 (2023), arXiv:2206.03343 [nucl-ex].

[74] V. Vovchenko, V. Koch, C. Shen, «Proton number cumulants and correlation functions in Au–Au collisions at $\sqrt{s_{NN}} = 7.7$–200 GeV from hydrodynamics», *Phys. Rev. C* **105**, 014904 (2022), arXiv:2107.00163 [hep-ph].

[75] X. Luo, J. Xu, B. Mohanty, N. Xu, «Volume fluctuation and auto-correlation effects in the moment analysis of net-proton multiplicity distributions in heavy-ion collisions», *J. Phys. G: Nucl. Part. Phys.* **40**, 105104 (2013), arXiv:1302.2332 [nucl-ex].

[76] B. Friman, V. Koch, «To bin or not to bin: does binning in multiplicity reliably suppress unwanted volume fluctuations?», arXiv:2511.11869 [nucl-th].

[77] A. Rustamov, J. Stroth, R. Holzmann, «A model-free procedure to correct for volume fluctuations in E-by-E analyses of particle multiplicities», *Nucl. Phys. A* **1034**, 122641 (2023), arXiv:2211.14849 [nucl-th].

[78] M.I. Gorenstein, M. Gazdzicki, «Strongly intensive quantities», *Phys. Rev. C* **84**, 014904 (2011), arXiv:1101.4865 [nucl-th].

[79] E. Sangaline, «Strongly Intensive Cumulants: Fluctuation Measures for Systems With Incompletely Constrained Volumes», arXiv:1505.00261 [nucl-th].

[80] Z. Wang, X. Luo, «A centrality-independent framework for revealing genuine higher-order cumulants in heavy-ion collisions», *Phys. Lett. B* **871**, 139984 (2025), arXiv:2505.03666 [physics.data-an].

[81] M. Stephanov, Y. Yin, «Hydrodynamics with parametric slowing down and fluctuations near the critical point», *Phys. Rev. D* **98**, 036006 (2018), arXiv:1712.10305 [nucl-th].

[82] L.D. Landau, E.M. Lifshitz, «Fluid Mechanics», vol. 6 of «Course of Theoretical Physics», *Butterworth-Heinemann*, Oxford, England 1987, 2nd ed.

[83] M.S. Pradeep, M. Stephanov, «Maximum Entropy Freeze-Out of Hydrodynamic Fluctuations», *Phys. Rev. Lett.* **130**, 162301 (2023), arXiv:2211.09142 [hep-ph].

[84] V.A. Kuznietsov *et al.*, «Critical point particle number fluctuations from molecular dynamics», *Phys. Rev. C* **105**, 044903 (2022), arXiv:2201.08486 [hep-ph].

[85] V.A. Kuznietsov, M.I. Gorenstein, V. Koch, V. Vovchenko, «Coordinate *versus* momentum cuts and effects of collective flow on critical fluctuations», *Phys. Rev. C* **110**, 015206 (2024), arXiv:2404.00476 [nucl-th].

[86] X. An *et al.*, «The BEST framework for the search for the QCD critical point and the chiral magnetic effect», *Nucl. Phys. A* **1017**, 122343 (2022), arXiv:2108.13867 [nucl-th].

[87] M. Pradeep, K. Rajagopal, M. Stephanov, Y. Yin, «Freezing out fluctuations in Hydro+ near the QCD critical point», *Phys. Rev. D* **106**, 036017 (2022), arXiv:2204.00639 [hep-ph].

[88] STAR Collaboration (M. Abdallah *et al.*), «Cumulants and correlation functions of net-proton, proton, and antiproton multiplicity distributions in Au+Au collisions at energies available at the BNL Relativistic Heavy Ion Collider», *Phys. Rev. C* **104**, 024902 (2021), arXiv:2101.12413 [nucl-ex]; *Erratum ibid.* **111**, 029902 (2025).

[89] STAR Collaboration (M. Abdallah *et al.*), «Higher-order cumulants and correlation functions of proton multiplicity distributions in $\sqrt{s_{NN}} = 3$ GeV Au+Au collisions at the RHIC STAR experiment», *Phys. Rev. C* **107**, 024908 (2023), arXiv:2209.11940 [nucl-ex].

[90] STAR Collaboration (B.E. Aboona *et al.*), «Precision Measurement of Net-Proton-Number Fluctuations in Au+Au Collisions at RHIC», *Phys. Rev. Lett.* **135**, 142301 (2025), arXiv:2504.00817 [nucl-ex].

[91] P. Braun-Munzinger *et al.*, «Relativistic nuclear collisions: Establishing a non-critical baseline for fluctuation measurements», *Nucl. Phys. A* **1008**, 122141 (2021), arXiv:2007.02463 [nucl-th].

[92] V. Vovchenko *et al.*, «Repulsive baryonic interactions and lattice QCD observables at imaginary chemical potential», *Phys. Lett. B* **775**, 71 (2017), arXiv:1708.02852 [hep-ph].

[93] B. Friman, K. Redlich, A. Rustamov, «Baselines for Abelian Charge Fluctuations in Nuclear Collisions:Theory and Comparison with Experimental Data», arXiv:2508.18879 [nucl-th].

[94] F. Reif, «Fundamentals of Statistical, Thermal Physics», *McGraw-Hill*, New York 1965.

[95] A. Mukherjee, J. Steinheimer, S. Schramm, «Higher-order baryon number susceptibilities: Interplay between the chiral and the nuclear liquid-gas transitions», *Phys. Rev. C* **96**, 025205 (2017), arXiv:1611.10144 [nucl-th].

[96] V. Vovchenko, L. Jiang, M.I. Gorenstein, H. Stoecker, «Critical point of nuclear matter and beam-energy dependence of net-proton number fluctuations», *Phys. Rev. C* **98**, 024910 (2018), arXiv:1711.07260 [nucl-th].

[97] A. Sorensen, V. Koch, «Phase transitions and critical behavior in hadronic transport with a relativistic density functional equation of state», *Phys. Rev. C* **104**, 034904 (2021), arXiv:2011.06635 [nucl-th].

[98] X. Zhang, Y. Zhang, X. Luo, N. Xu, «UrQMD simulations of higher-order cumulants in Au+Au collisions at high baryon density», *Chin. Phys. C* **50**, 011003 (2026), arXiv:2506.18832 [nucl-ex].

[99] STAR Collaboration (Z. Sweger), «Proton high-order cumulants results from the STAR fixed-target program», presented at Quark Matter 2025, Frankfurt, Germany, 2025, https://indico.cern.ch/event/1334113/contributions/6369534/attachments/3048338/5386843/QM2025_Sweger_v64.pdf

[100] A. Bzdak, V. Koch, V. Vovchenko, «Acceptance dependence of factorial cumulants, long-range correlations, and the antiproton puzzle», *Phys. Rev. C* **112**, 024901 (2025), arXiv:2503.16405 [nucl-th].

[101] A. Bzdak, V. Koch, V. Skokov, N. Strodthoff, «Cumulants *vs* correlation functions and the QCD phase diagram at low energies», *Nucl. Phys. A* **967**, 465 (2017).

[102] A. Bzdak, V. Koch, V. Skokov, «Correlated stopping, proton clusters and higher order proton cumulants», *Eur. Phys. J. C* **77**, 288 (2017), arXiv:1612.05128 [nucl-th].

[103] A. Bzdak, V. Koch, «Rapidity dependence of proton cumulants and correlation functions», *Phys. Rev. C* **96**, 054905 (2017), arXiv:1707.02640 [nucl-th].

[104] S.A. Bass, P. Danielewicz, S. Pratt, «Clocking Hadronization in Relativistic Heavy-Ion Collisions with Balance Functions», *Phys. Rev. Lett.* **85**, 2689 (2000), arXiv:nucl-th/0005044.

[105] S. Jeon, S. Pratt, «Balance functions, correlations, charge fluctuations, and interferometry», *Phys. Rev. C* **65**, 044902 (2002), arXiv:hep-ph/0110043.

[106] C. Pruneau *et al.*, «Accounting for nonvanishing net-charge with unified balance functions», *Phys. Rev. C* **107**, 014902 (2023), arXiv:2209.10420 [hep-ph].

[107] H. Heiselberg, «Event-by-event physics in relativistic heavy-ion collisions», *Phys. Rep.* **351**, 161 (2001), arXiv:nucl-th/0003046.

[108] STAR Collaboration (J. Adams *et al.*), «Incident energy dependence of $p_t$ correlations at relativistic energies», *Phys. Rev. C* **72**, 044902 (2005), arXiv:nucl-ex/0504031.

[109] K.-J. Sun, L.-W. Chen, C.M. Ko, Z. Xu, «Probing QCD critical fluctuations from light nuclei production in relativistic heavy-ion collisions», *Phys. Lett. B* **774**, 103 (2017), arXiv:1702.07620 [nucl-th].

[110] D. DeMartini, E. Shuryak, «Many-body forces and nucleon clustering near the QCD critical point», *Phys. Rev. C* **104**, 024908 (2021), arXiv:2010.02785 [nucl-th].

[111] Y. Akamatsu *et al.*, «Enhancement of photon emission rate near QCD critical point», *Phys. Rev. D* **113**, 034009 (2026), arXiv:2505.07169 [hep-ph].

[112] R.A. Lacey, «Indications for a Critical End Point in the Phase Diagram for Hot and Dense Nuclear Matter», *Phys. Rev. Lett.* **114**, 142301 (2015), arXiv:1411.7931 [nucl-ex].

[113] A. Sorensen, P. Sorensen, «Locating the critical point for the hadron to quark–gluon plasma phase transition from finite-size scaling of proton cumulants in heavy-ion collisions», arXiv:2405.10278 [nucl-th].